Surface species formed by the adsorption and dissociation of water molecules on a Ru(0001) surface containing a small coverage of carbon atoms studied by scanning tunneling microscopy

Tomoko K. Shimizu,[1, 2] *Aitor Mugarza,*[1,3] *Jorge I. Cerdá,*[4] *Markus Heyde,*[1+]

Yabing Qi,[1,5] *Udo D. Schwarz,*[6] *D. Frank Ogletree,*[1] *Miquel Salmeron*[1,2*]

1 . Materials Sciences Division, Lawrence Berkeley National Laboratory, Berkeley, CA 94720, USA

2. Department of Materials Science and Engineering, University of California at Berkeley, CA 94720, USA

3. Institut de Ciencia de Materials de Barcelona, CSIC, Bellaterra, 08193 Barcelona, Spain

4. Instituto de Ciencia de Materiales de Madrid, CSIC, Cantoblanco, 28049 Madrid, Spain

5. Applied Science and Technology, University of California at Berkeley, CA 94720, USA

6. Department of Mechanical Engineering, Yale University, P.O. Box 208284, New Haven, CT 06520-8284, USA

+Current address: Department of Chemical Physics, Fritz-Haber-Institut der Max-Planck-Gesellschaft, Faradayweg 4-6, D-14195 Berlin, Germany

MBSalmeron@lbl.gov

*CORRESPONDING AUTHOR FOOTNOTE

Telephone number: +1-510-486-6230. Fax number: +1-510-486-7268. E-mail: MBSalmeron@lbl.gov

Abstract: The adsorption and dissociation of water on a Ru(0001) surface containing a small amount (≤ 3 %) of carbon impurities was studied by scanning tunneling microscopy (STM). Various surface species are formed depending on the temperature. These include molecular H_2O, H_2O-C complexes, H, O, OH and CH. Clusters of either pure H_2O or mixed H_2O-OH species are also formed. Each of these species produces a characteristic

contrast in the STM images and can be identified by experiment and by *ab initio* total energy calculations coupled with STM image simulations. Manipulation of individual species via excitation of vibrational modes with the tunneling electrons has been used as supporting evidence.

1. Introduction

The adsorption of water on surfaces is a topic of long standing interest in electrochemistry, catalysis and environmental sciences.[1,2] In all these fields, determining the nature of the species formed upon adsorption of water is a crucial first step for an understanding of the chemical process and for the development of predictive models of reactivity and wetting characteristics of the material. The expected species include intact molecules (H_2O), hydroxyls (OH), oxygen (O), hydrogen (H), in addition to reaction and solvation products with other surface atoms. The scanning tunneling microscope (STM) is an excellent tool to study the structure and spatial distribution of these species. Precise identification of different species by STM is, however, challenging because the observed image contrast depends on their detailed composition and electronic structure as well as that of the tip.

In the past decade, inelastic electron tunneling spectroscopy (IETS) by STM has brought the capability of chemical identification through vibrational spectroscopy to the single molecular level.[3] When molecular vibrational modes are excited by tunneling electrons, anharmonic effects can couple the modes and induce molecular motions or reactions such as diffusion and dissociation. Examples of these effects include the diffusion of water molecules on Pd(111),[4] Cu(111) and Ag(111),[5] after excitation of the scissor or O-H stretch modes by tunneling electrons. In these cases, although it is difficult to obtain IET spectra, chemical information can be extracted by investigating the vibrationally induced processes. We have made a detailed study of these effects for water and its dissociation products on Ru(0001). While a full report will be presented in a forthcoming article, some results will be briefly mentioned here when needed to support the identification of surface species. In this paper, we present a study of the various species formed upon water adsorption and dissociation on Ru(0001). *Ab initio* calculations of the structure and energetics of these species, together with STM image contrast calculations, are also presented. In addition to helping the interpretation they provide a deeper understanding of the origin of the contrast mechanism in each case. Density Functional Theory (DFT) provided the adsorption geometry and electronic structure. Simulated STM images were obtained by explicitly taking into account the

tip-sample coupling.[6] A theoretical analysis of the appearance of various atomic adsorbates on Pd(111) was presented by Tilinin et al.[7] They found that atomic size and electronegativity were among the factors that determined the STM image contrast. Small species that subtract electron density from the Fermi level of the metal (by forming filled bonding orbitals well below the Fermi level), such as H, O and C, typically lead to a decrease in tunneling probability that produces negative contrast or depressions in STM images. For intermediate cases, where contribution of the atomic size and electronegativity are of the same order, the appearance can be more complex, such as protrusions surrounded by a depression ring. Finally, if the atomic size is large enough to overcome the apparent depression cased by the electronegativity of the species, they appear as protrusions in the images. From the theoretical point of view, our system presents a challenging case where different species coexist on the same surface, often with subtle differences among them. In order to reproduce the shape and corrugation of *all* the species imaged under the same tip and tunneling conditions, we have additionally explored a wide variety of tip apex structures.

The Ru surface used in these studies contained a certain amount of carbon (C) impurities (< 0.03 ML), with which water interacts to give a rich variety of species and complexes. Determination of the nature of such C-related species adds to our

fundamental knowledge of the chemistry and catalytic role of Ru in important reactions such as Fischer-Tropsch.

2. Experimental

(a) Instrumentation

The experiments were performed using a home-built STM controlled by commercial RHK electronics. The system consists of two ultra-high vacuum (UHV) chambers connected to each other, as shown in the schematic diagram of Figure 1 (a). One contains standard instrumentation for sample preparation and characterization, including low energy electron diffraction (LEED), Auger electron spectroscopy (AES), mass spectrometry and ion sputtering. The other chamber holds a commercial cryostat from CryoVac,[8] with liquid nitrogen and liquid helium reservoirs. The STM head, shown in Figure 1 (b) and (c) is based on the design of Pan et al.[9] where the coarse approach is achieved by the slip-stick motion of the scanner using a set of shear piezos. The sample is mounted on top of the scanner and the tip is stationary. The tip and the sample can be exchanged using a wobble stick. The sample can be heated from 6 to 300 K in the STM with a resistor mounted near the sample plate. The sample temperature is measured by a Si diode mounted between the sample plate and the heater. In the present experiments the

sample was annealed at different temperatures to induce chemical changes and then cooled back to 6 K for imaging.

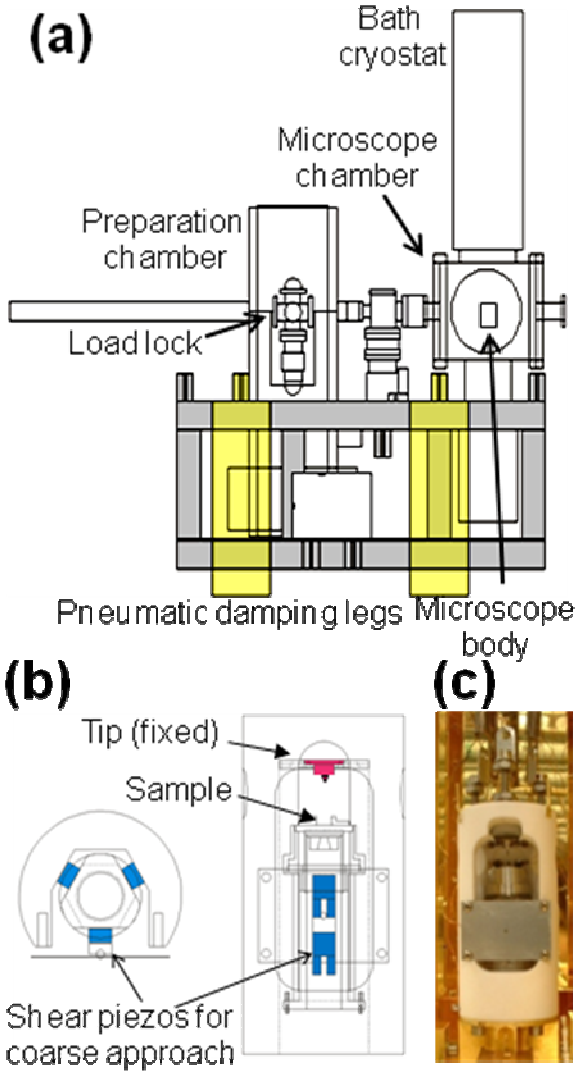

Figure 1.

(b) Sample preparation

The single crystal Ru(0001) sample was initially cleaned by several cycles of Ar^+ sputtering at 1 keV and annealing to 1500 K by electron-bombardment. After the sputter-anneal cycles or after each STM experiment, it was repeatedly heated and cooled

from 750 K to 1500 K in an O_2 atmosphere of 1-2 × 10^{-7} Torr. Finally it was flash-annealed to 1650 K in UHV in order to remove excess O from the surface, as confirmed by AES spectra that show no O peak within the experimental resolution. Occasionally a small O peak (corresponding to a very small fraction of a monolayer) was detected in spectra taken approximately 30 minutes after preparation. The presence of small amounts of C is difficult to determine by AES because the C peak at 272 eV overlaps with the main Ru peak at 273 eV. Its presence however is easily detected by STM, as shown in the image of Figure 2. The dark spots in this image are due to C atoms, which segregate from the bulk after the high temperature flash-annealing. We will discuss the experimental evidence supporting this assignment in more detail below. The C surface concentration was approximately 3 % of a monolayer (ML), as found by counting spots and using the Ru surface atom density. Although the visual appearance of the image gives the impression of a higher coverage of C, that is simply due to the relatively large footprint of the C depression by convolution with the STM tip. As shown later, the length of the tip trace as it scans over the atom is around 1 nm, about 3 times the lattice distance in Ru. It should be noted that the observed C atoms in the STM images cannot be due to e-beam assisted deposition during the AES measurement since after that the same cleaning procedure was repeated before STM measurement.

Milli-Q water in a glass tube was degassed by repeated cycles of freezing, pumping, and thawing prior to being introduced into the chamber through a leak valve and a dosing tube pointing towards the sample. After dosing, the sample was heated to various temperatures in order to induce reactions and rearrangements of H_2O and other species.

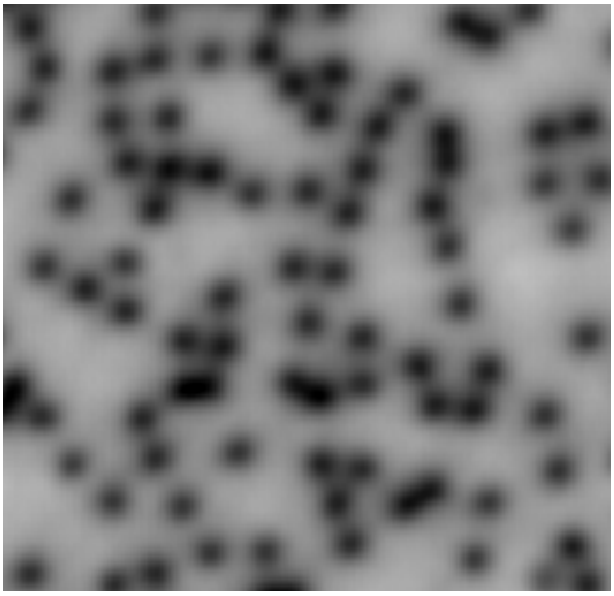

Figure 2.

(c) Tip preparation

All STM data were collected at 6 K at a base pressure below 2×10^{-11} Torr, using electrochemically etched W tips. The tips were further prepared *in-situ* by field emission and by voltage pulses and/or controlled contacts with the surface, until sharp and symmetric images of surface adsorbates were obtained. The final nature of the tip apex, however, could not be systematically controlled and the contrast and lateral resolution varied in images taken with different tips. The images obtained can be classified into

three types that we associate with blunt, sharp, and anomalous tips. The blunt tips do not resolve the very small corrugation of the Ru lattice and are believed to consist of multiple atoms at the apex participating in the tunneling process. In contrast sharp tips, which we believe to have a single atom termination, do resolve the Ru lattice with a corrugation of ~2 pm (noise level is ~0.5 pm) at gap resistances around 10^8 Ohm or less, as shown in Figure 3 (a). They also produce the sharpest images of atoms and molecules. Such tips could be obtained after a gentle contact with the Ru surface. After this contact a bump was observed in subsequent images of the area of the contact, suggesting that the tip structure was produced by transfer of a small amount of tip material to the surface. Finally anomalous tips, which occurred more rarely, produced unexpectedly high Ru lattice corrugation (3-8 pm), as shown in Figure 3 (b). These tips are believed to have an atom or molecule attached to the apex, as they were produced (although not very reproducibly) after exposure to gases such as H_2O and H_2 or by applying small voltage pulses to capture adsorbed species. While such tips are useful for determining adsorption sites and coverage, their unknown structure made them unsuitable for comparison with theoretical image simulations. Only the sharp tip images were used for that purpose.

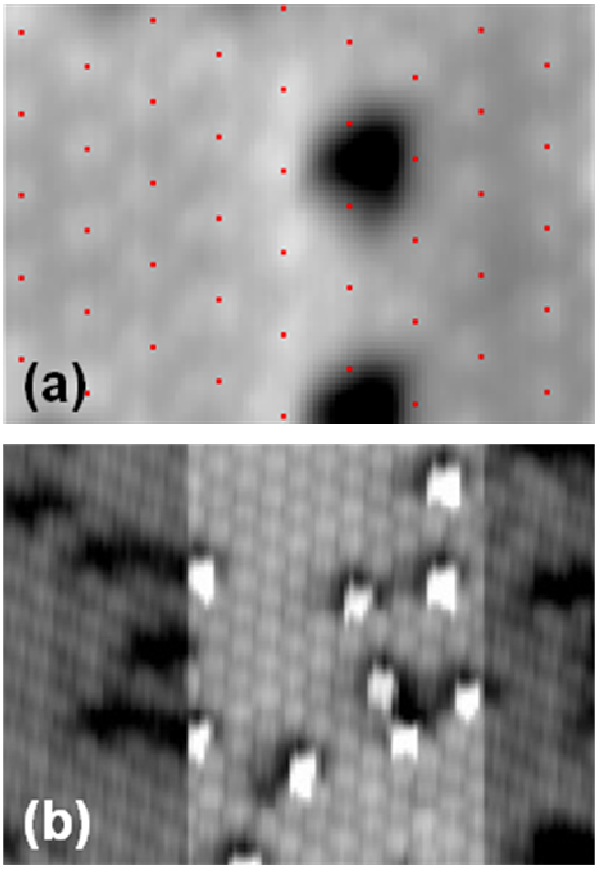

Figure 3.

3. Theoretical modeling

To simulate STM images a three-step procedure was followed.[10,11] First, DFT calculations were performed to obtain the optimized geometry and electronic structure for a given adsorption model and for different tip structures. Second, a parametrization of the semi-empirical Hamiltonian of the Extended Hückel Theory (EHT) was performed by fitting the DFT derived electronic density of states (DOS) projected onto the surface atomic orbitals (AOs). Third and finally, an infinite system composed of two semi-infinite blocks for the tip and the sample was constructed, employing the

parameterized EHT to describe all electronic interactions, and used to calculate the tunneling current.

The DFT calculations were performed using the SIESTA package[12] under the generalized gradient approximation (GGA).[13] Isolated species or complexes were modeled by slab geometries containing 3 Ru layers along the [0001] direction with a p(4 × 4) unit cell. We used standard parameter values for k-sampling, AO basis and other SIESTA specific parameters, and checked that the results were hardly modified upon increasing the convergence criteria. The binding energies deduced from the present calculations are listed in Table 1 for all the structures considered. Although the reported adsorption energies may deviate from the experimental values due to the multiple approximations involved, the qualitative trends can be reliably extracted from the table (e.g., the energetic hierarchy among different adsorption sites for a given species).

Table 1.

Species	hcp	fcc	Top
O	7.84	7.59	
C	9.05	8.64	
H	4.07	4.10	
CH	7.63	7.42	5.92
OH	4.24	4.22	3.31

H_2O	[b]	0.36	0.70
H_2O-C [a]			9.85

To model the tip apex we considered several pyramidal clusters stacked on periodic, un-relaxed W-bcc slabs oriented either along the [110] or [111] directions. We also modeled a [111] W-fcc slab since it provides a sharper apex than the W-bcc. In order to minimize apex-apex interactions, we used a p(4 × 4) unit cell for these DFT calculations. The clusters typically contained 10 to 14 atoms, also allowing for the presence of C, O, CH or H species. We will only present here results obtained with a W-fcc (111) oriented tip with a sharp 10 atom pyramidal termination because this tip reproduced best the images obtained with the experimental sharp tips described above. We cannot rule out, however, that other tip structures could give similar results.

A fit of the EHT parameters to reproduce the SIESTA derived DOS was then performed for each *ab initio* calculation on each model system.[10] We employed a single-zeta basis set for all elements, with each *l*-shell described by one or two Slater orbitals. The only exception was the water molecule, for which we added a second s orbital to the H in order to account for the lowest and next lowest unoccupied molecular orbitals, the LUMO and LUMO+1, respectively. Figure 4 illustrates the level of

agreement obtained with the EHT fit for this case by showing the projected DOS (PDOS) onto the water molecule and the Ru atom below it. Similar or better agreement has been obtained for the other atoms in the slab and for the rest of systems considered. A decomposition of the water EHT-PDOS into its MO contributions is also presented in the figure. By inspecting the broadening of these states, one may deduce that the highest occupied MO (HOMO) and the LUMO+1 show the largest interactions with the Ru atoms (states $1B_1$ and $2B_2$). An excellent correspondence between the SIESTA and EHT calculations is obtained except for the LUMO+1 state. Given the poor reliability of DFT for describing unoccupied states, we do not feel that this discrepancy is significant. Furthermore, the EHT provides a larger gap between the $1B_1$ and $2B_2$ MOs, which should partly correct the too-small gaps typically obtained with GGA.

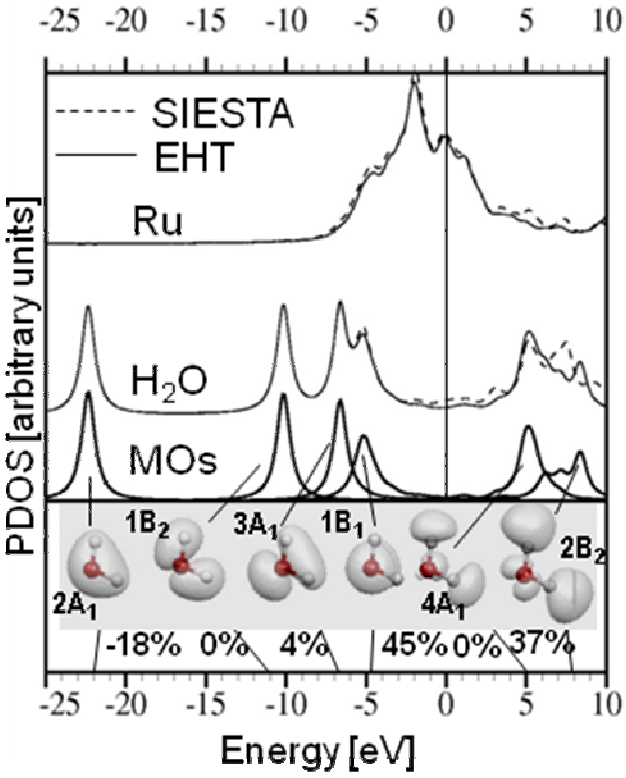

Figure 4.

In the last step, the DFT optimized geometries for the surface and tip apex atoms are each attached to Ru(0001) and W bulk slabs to construct the sample and tip blocks. After independently solving the Green's function for each surface, the two semi-infinite blocks are brought close to each other and matched up to first order in the apex-surface interactions in order to calculate the elastic tunneling current flowing between tip and sample.[11] In the matching process, a rigid shift between the tip and sample Fermi levels of eV_{tip} was imposed for a given bias V_{tip}. Topographic images were simulated by repeating the matching process while scanning the tip over the entire (4 × 4) surface cell with 50 pm resolution. At each pixel the tip height was adjusted until the desired current was

achieved. We fixed the tunneling parameters in all cases to V_{tip} = 100 mV and I = 0.2 nA following the typical experimental conditions. Apparent heights and shapes of species derived in this way are summarized in Table 2, together with experimental ones for comparison.

Table 2.

Species	Site	Blunt tip	Sharp tip	
		Experiment		Theory [a)]
C	hcp	35-45 pm round depression	~45 pm triangular depression	23 pm triangular depression
O	hcp	35-45 pm round depression	~70 pm round depression	48 pm round depression
H_2O	top	50-65pm round protrusion	~55 pm round protrusion	51 pm round protrusion
H_2O-C	top-hcp	20-35 pm protrusion and 10-20 pm depression	~30 pm protrusion and ~20pm depression	37 pm protrusion and 17 pm depression
H	fcc	10-25 pm round depression	~35 pm slightly triangular depression	15 pm slightly triangular depression
CH	hcp	15-25 pm round depression	~25 pm triangular depression with a center maximum	18 pm triangular depression with a center maximum
OH	hcp	3-10 pm round protrusion	~10 pm round protrusion surrounded by ~2 pm deep ring	11 pm round protrusion surrounded by 13 pm deep ring

4. Results and Discussion

(a) Ru(0001) surface before water adsorption

Figure 2 shows a typical STM image of the as-prepared Ru(0001) surface. The Ru atoms lattice is not resolved in this large image obtained with a blunt tip. Many circular 35-45 pm depressions (dark spots) are visible due to impurity atoms. The width and depth of the spots did not depend on tunneling parameters, within the range used in our experiments: V_{sample} = ±25 to 1000 mV, I_t = 0.05 to 2 nA. The impurity concentration was approximately 0.03 ML. Sometimes the impurities formed small aggregates, with a minimum separation of two Ru lattice constants.

The most likely atoms responsible for the dark spots are C and O. No other species, such as sulfur, was detected by AES. Carbon is a main bulk impurity of Ru and oxygen is used during sample cleaning. By adsorbing O_2 at 25 K, which dissociates upon adsorption on Ru(0001),[14-17] we could obtain reference images of O atoms. With blunt tips the adsorbed O atoms appear also as circular depressions ~45 pm deep and thus are difficult to distinguish from the preexisting dark spots, as shown in Figure 5 (a). However with sharp tips the oxygen atoms produce circular depressions ~70 pm deep while the initial impurities, which we assign to C atoms, produce triangular shaped depressions ~45 pm

deep. Simulated sharp tip STM images and height profiles of C and O atoms, shown in Figures 5 (c) and (d), support this assignment. The experimentally observed contrast: triangular depressions for C and deeper, symmetric depressions for O, are well reproduced. Although the relative depths for C and O are consistent, the calculated depths are smaller by a factor of ~2 for C and ~1.5 for O. Such quantitative disagreement is not surprising due to multiple approximations involved in the STM theoretical formalism and the fact that the precise apex structure is unknown.

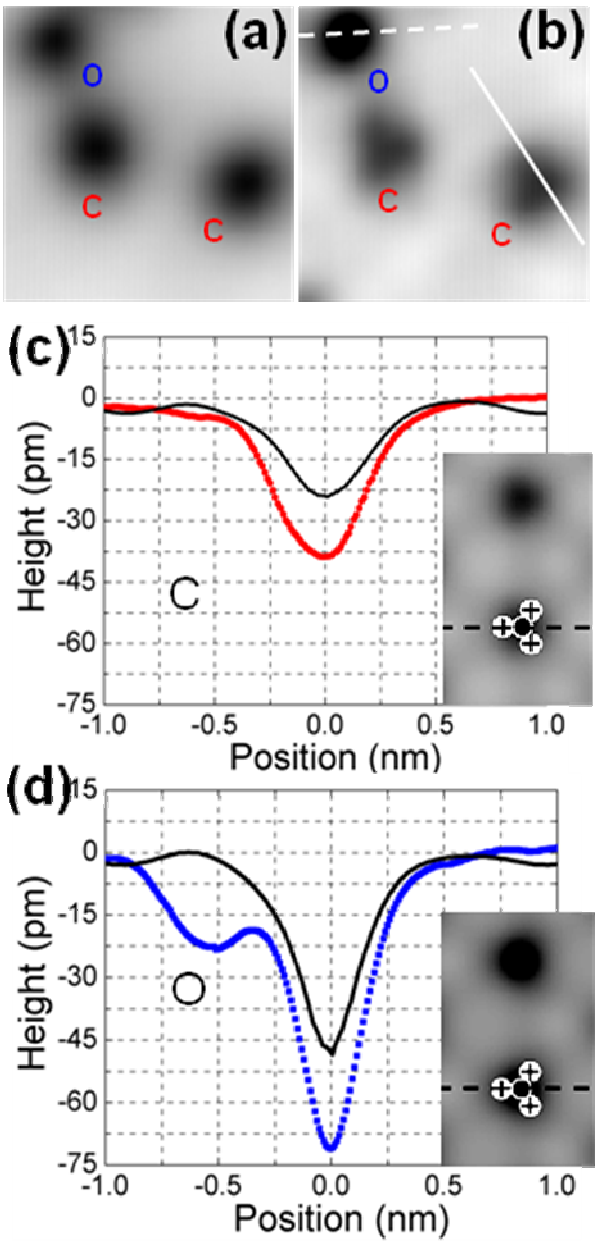

Figure 5.

We have also confirmed through image simulations that the tip sharpness is indeed responsible for the contrast difference between Figure 5 (a) and (b). For blunt tips the depressions become rounded and shallower, closely resembling those shown in Figure 5 (a). A decomposition of the current in terms of adsorbate and substrate contributions[18]

reveals that the triangular shape of the C atoms in the images is the result of direct tunneling into the surrounding Ru atoms, whose electronic structure is strongly perturbed by presence of the C. We also note that the orientation of the triangular shape of C in the images is inverted with respect to the triangle of 3 Ru atoms around the hollow site (Figure 3 (a)). Similar shapes have been reported for O on several metal surfaces,[18,19] although in many cases the triangle orientation was the opposite.

Atomically resolved images of the Ru surface lattice, like those in Figure 3, indicate that both O and C atoms occupy the same type of hollow sites. The DFT results, presented in Table I, are in line with this finding since they predict the hcp hollow site as the preferential adsorption site for both C and O.

(b) H_2O monomers

In order to study individual H_2O molecules, approximately 0.004 ML of H_2O was adsorbed on the surface at 25 K and imaged at 6 K. The STM images revealed new bright features or protrusions with a density that increased in proportion to water vapor exposure. They were therefore assigned to intact water monomers. It is known that water does not dissociate on Ru(0001) at this temperature.[20,21]

Two types of protrusions with different heights were observed, as shown in Figure 6 (a) and (b). The higher ones are due to isolated molecules, defined as being at least 2 lattice

distances away from any C impurity; the lower ones are due to water molecules on top sites next to hollow-site C atoms. In both cases, water adsorbs on top site, which was also confirmed by DFT calculation. A close-up view of an isolated water molecule obtained with a sharp tip is shown in Figure 6 (c), together with a calculated image in (d). Despite H_2O being a closed shell system there is a substantial broadening of the $1B_1$ and $2B_2$ MOs due to their interaction (see Figure 4), which leads to a non negligible H_2O PDOS at the Fermi level, favoring direct tunneling into the molecule and giving a positive contrast. In Figure 4, we indicate the percentage contribution of each MO to the total current when the tip is placed on top of the monomer. As expected, the HOMO dominates approximately half the current (45 %). Indeed, the rounded shape of the $1B_1$ HOMO is reflected in both the theoretical and experimental images. There is also a comparable contribution from the LUMO+1 (37 %) and more surprisingly, a negative contribution (–18 %) from the $2A_1$ state despite its being located well below the Fermi level. Similar negative contributions from deep states have been previously reported for other molecules[23] and are clearly due to interference effects in the electron tunneling process. The contributions of these two latter MOs somewhat distorts the circular symmetry of the H_2O bump, as can be seen both in the theoretical and experimental images. The remaining 32 % of the contribution to the tunneling current not indicated in Figure 4 is due to direct tunneling into the six Ru atoms

surrounding the one directly bound to the water molecule. As shown in the experimental and theoretical line profiles in Figure 6 (e), the typical apparent height of isolated water is 50-65 pm. The width (FWHM) varies from 0.28 nm with sharp tips to 0.70 nm with blunt tips. Different tunneling parameters did not appreciably change the apparent height. These dimensions are similar to those found for water monomers on other metal surfaces.[24-26] By drawing a 1 × 1 grid of Ru atom sites (using the C impurities and atomically resolved images as references), the monomers were found to always adsorb on top sites.

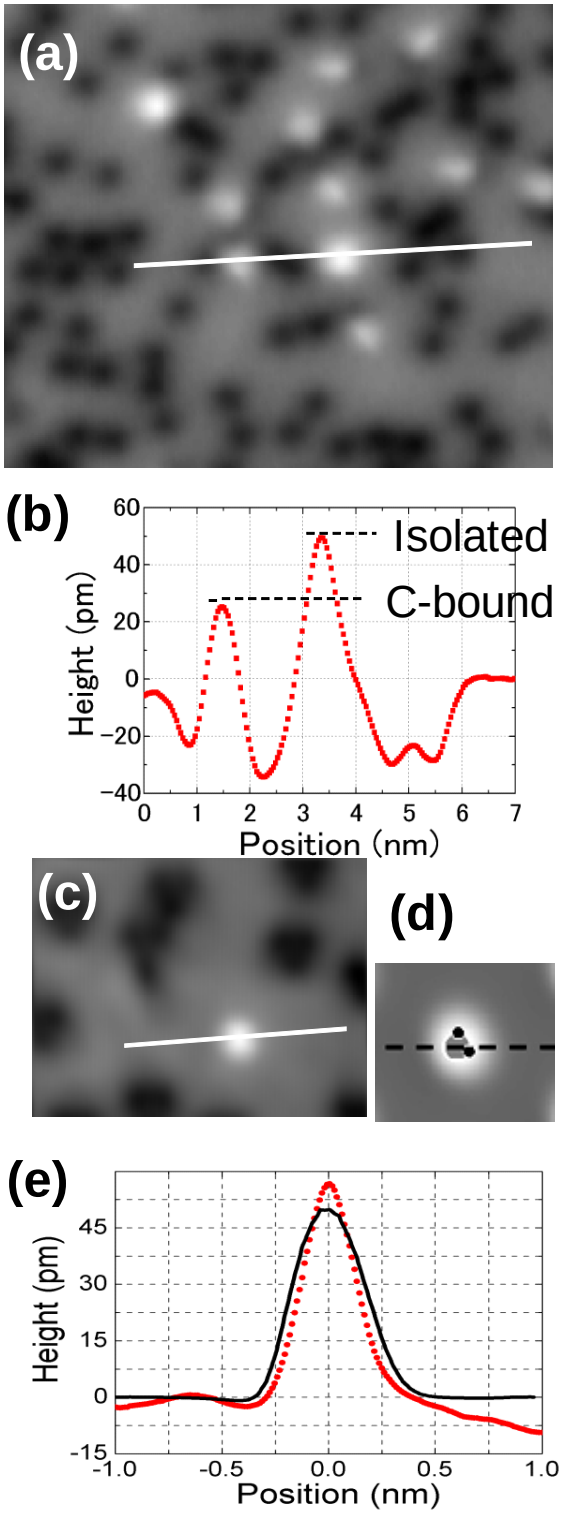
(a)
(b)
Isolated
C-bound
Height (pm)
Position (nm)
(c)
(d)
(e)
Height (pm)
Position (nm)

Figure 6.

The second type of protrusions, also due to water on top sites, has a reduced height of 20-35 pm. A height profile along the two types of water molecules is shown in Figure 6 (b). These lower-contrast molecules are always found adjacent to C atoms. Because of the substantial overlap of the C and H_2O profiles, it is difficult to determine the exact adsorption site of water in these images. Fortunately, by applying voltage pulses with the tip, we could displace the H_2O molecule from the C, thus allowing for an accurate measure of the in-plane H_2O-C distance, as shown in the images of Figure 7 (a) and (b). Although not shown here, by using the same procedure we could reversibly convert one type of water molecule into the other. Topographic profiles obtained before and after displacement of the molecule (Figure 7 (c)) give an average C-H_2O separation of 0.32 ± 0.03 nm (0.31 nm in the figure), which matches within experimental error the distance between the top site and the second nearest hollow Ru lattice site of 0.31 nm. Knowing that water adsorbs with its plane nearly parallel to the surface,[27] we propose the configuration illustrated in Figure 7 (d) for the H_2O-C complex. After annealing to 100 K, no isolated water molecules were observed, all having moved to form complexes with C atoms or to form clusters with other water molecules nucleated around C impurities. This reflects the attractive nature of the H_2O-C interaction.

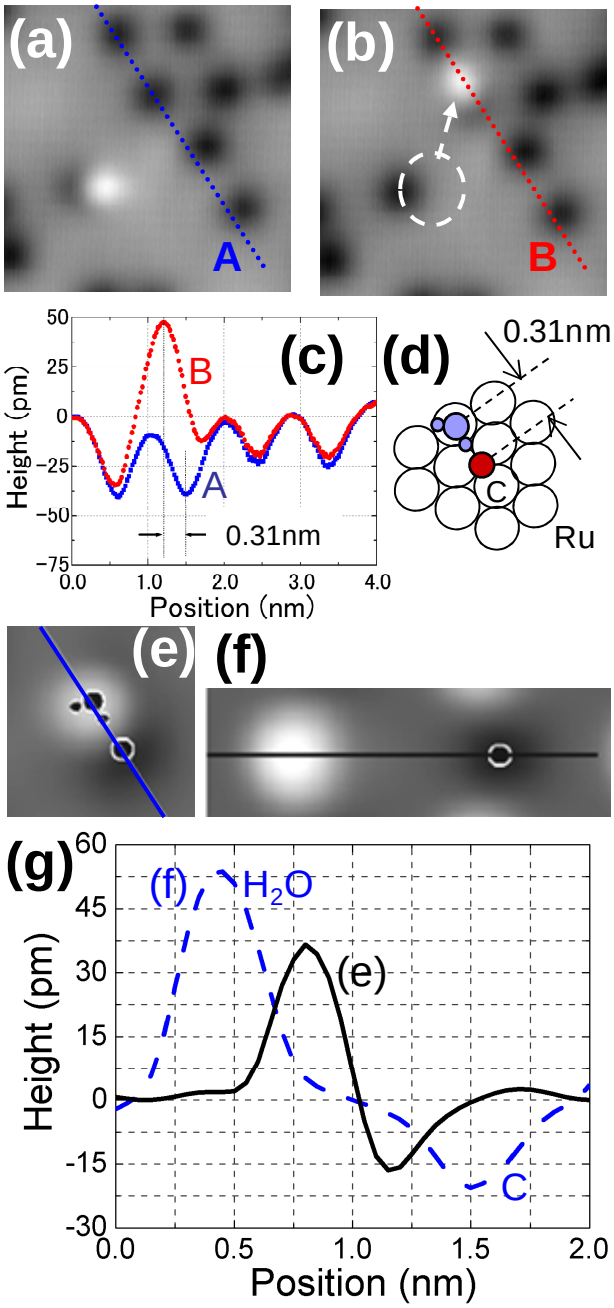

Figure 7.

In agreement with this finding, total energy calculations indicate that the H_2O-C complex is more stable than coadsorbed C and H_2O in a non-bonding configuration by 100 meV – see Table I. The optimized geometry of the H_2O molecule corresponds to a

molecular plane nearly parallel to the surface, as drawn in Figure 3 (d), even in the complex. This also involves small lateral shifts (around 30 pm) of the O atoms from its respective top site towards C, with an O (H_2O)-C distance of 310 pm. The large H-C bond distance of 220 pm suggests that the stabilization mechanism is analogous to a hydrogen bond. Interestingly, the reduction in contrast height from isolated to C-bound H_2O in the images cannot be explained by a simple superposition of the maximum due to water and the minimum due to C. Using the experimental values as a reference, a reduction as large as 30 pm in the monomer apparent height would occur only if the water molecule occupied the same site as the C atom which, as shown above, is not the case. This is a clear indication of bond formation between C and H_2O despite the large interatomic distance[28] and excludes a pure van der Waals bonding mechanism. The STM simulations and height profiles for the H_2O-C complex as well as for a non-bonding system are presented in Figure 7 (e)-(g), respectively. In approximate agreement with the experiment, we obtain a 20 pm decrease in the height of the water molecule in the H_2O-C complex. A detailed comparison between the H_2O PDOS for the bonding and non-bonding configurations (not shown) reveals that the formers suffer an overall upshift in energy of only 0.2 eV while the C PDOS remains essentially unchanged. Most important is, however, the contraction of the 1s AO of the H bound to the C, leading to

more localized MOs and a corresponding decrease in tunneling current. Therefore, the reduction in the height of the protrusions upon formation of the H_2O-C complex is an electronic effect arising from the covalent character of the HOH-C bond, and reveals a high sensitivity of the STM to detect hydrogen bonds.

(c) Surface species formed by thermal dissociation of water

When the Ru surface was annealed to 140 K or above, three new species were formed as a result of the partial dissociation of H_2O. Two of these are observed outside the clusters of water molecules, as shown in Figure 8 (a). One is a 35 pm depression, approximately 0.30 nm wide in images obtained with sharp tips, which is easily differentiated from C or O. It was identified as H by comparison with images obtained after adsorption of H from pure H_2 gas. DFT calculations (Table 1) predict H adsorption in fcc hollow sites. Experimentally, the fcc nature of the site was confirmed by extending a 1 × 1 grid of points onto Ru sites by using the C sites as references. The assignment also agrees with previous theoretical[27,29] and experimental results obtained by LEED[30,31] and STM.[32] The simulated image of H (Figure 8 (b) inset) is a small roughly triangular shaped 15 pm depression and is a result of direct tunneling into Ru states. The triangle is oriented opposite to that formed by the neighboring Ru atoms. Although the calculated contrast for

H is smaller than the experimental one by a factor of 2 (Figure 8 (b)), the trend of increasing depth from H to C, to O is fully consistent with the experiments.

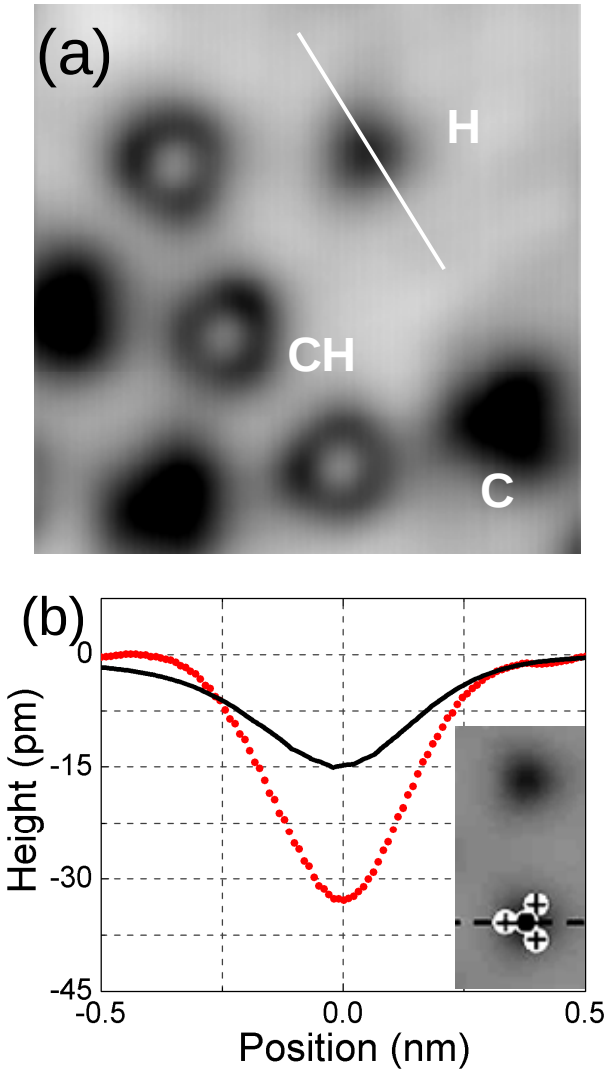

Figure 8.

In addition to isolated H atoms, another species can be found that appears as a circular depression 0.60 nm in diameter with a maximum at the center (sombrero shape), in images obtained with sharp tips, as shown in Figure 8 (a) and 9 (b). With blunt tips it appears as a depression 15-25 pm shallower than C, as shown in Figure 9 (a). We assign

this species to CH based on theoretical calculations (Figure 9 (c)) and the observation that it can be dissociated back into C and H by voltage pulses from the STM tip. The same CH species can also be produced in the absence of water by exposing the surface directly to H_2 gas molecules, which readily dissociate (at the adsorption temperature of the experiment of 100 K) to form adsorbed H. We find that C and CH have equivalent adsorption sites and the DFT total energy results presented in Table I confirm that the most energetically favorable site of CH is the hcp hollow, with the C-H bond vertical.

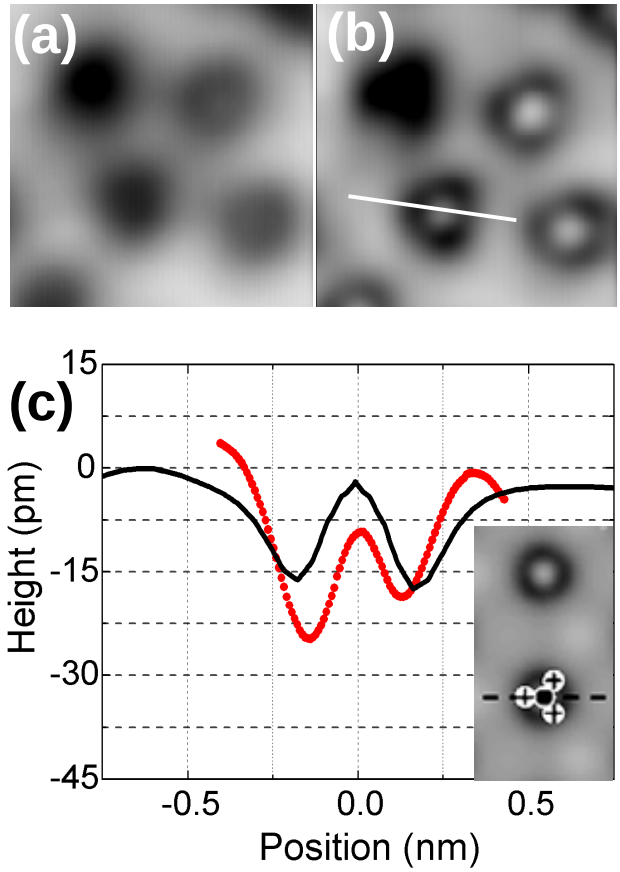

Figure 9.

A remarkable observation from these water thermal dissociation experiments is the absence of isolated O atoms or OH molecules. This indicates that the dissociation takes place inside the water clusters, which originally consisted of pure water molecules. Indeed the structure of the clusters changed substantially, becoming flatter and with a peculiar high contrast (bright) periphery, as shown in Figure 10. With sharp tips the internal structure of the clusters can be resolved and seen to consist of hexagonal units. Since no isolated OH or O could be observed, it follows that these species must be located inside the new clusters, which must then consist of mixtures of H_2O and OH, and perhaps also O. A detailed analysis to be presented soon in another paper suggests that the clusters consist of a mixture of H_2O and OH with all O-H bonds parallel to the surface.

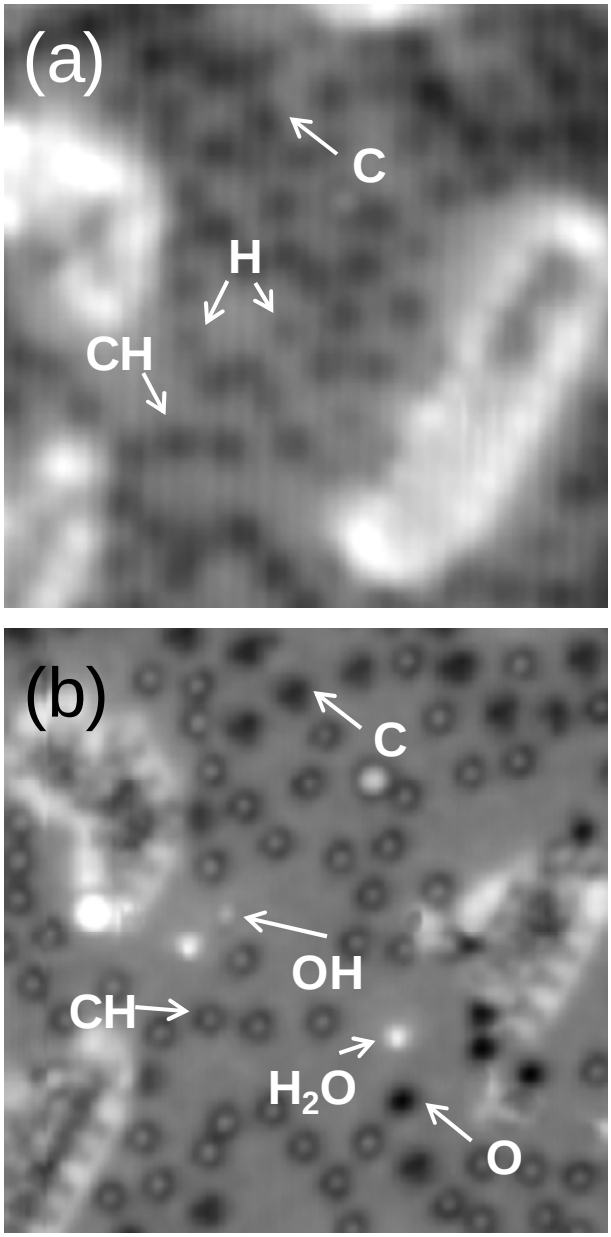

Figure 10.

(d) Formation of isolated OH molecules using tip manipulation techniques

Although thermal treatment did not generate isolated OH, these could be produced using the tip and the tunneling electrons to either separate the cluster into its constituents or to directly dissociate the molecules. In the example shown in Figure 10, the tip was

repeatedly scanned over the cluster on the right of the image with a sample bias of 0.5-0.7 V. As a result, isolated water molecules, OH molecules and O atoms were produced by the disassembly of the cluster as well as by the dissociation of H_2O and/or OH. In this experiment the tip changed structure during manipulation form blunt, in (a), to sharp, in (b), possibly functionalized by picking up a molecule. We also found that voltage pulses of 1 volt or higher applied when the tip is over a water molecule produced OH and H. This and other tip-induced effects will be discussed in detail elsewhere.

Figure 11 (a) shows two OH molecules produced by dissociation of water molecules. They are imaged as ~10 pm high protrusions. The H atom produced during dissociation was usually not found on nearby sites due to its easy diffusion when excited by tip voltages as low as 80 mV. Using the lattice extrapolation technique described above for the other species, we determined that the adsorption site of OH is the hcp hollow, although it could occasionally be displaced to fcc or bridge sites during manipulation experiments. The DFT results are in line with these observations: we obtain similar adsorption energies for OH at the hcp and fcc hollow sites (Table I) while adsorption on top sites is clearly unfavorable. The inset in Figure 11 (b) shows a simulated OH image. Like CH, OH appears as a shallow depression with a bump at the center, but the 3-fold symmetry is not present in OH. The dark ring surrounding the bump, clearly visible in

simulated images, is difficult to see in the experimental images due to its smaller contrast, as shown in the height profile in Figure 11 (b). The calculated image exhibits also a slightly higher central protrusion.

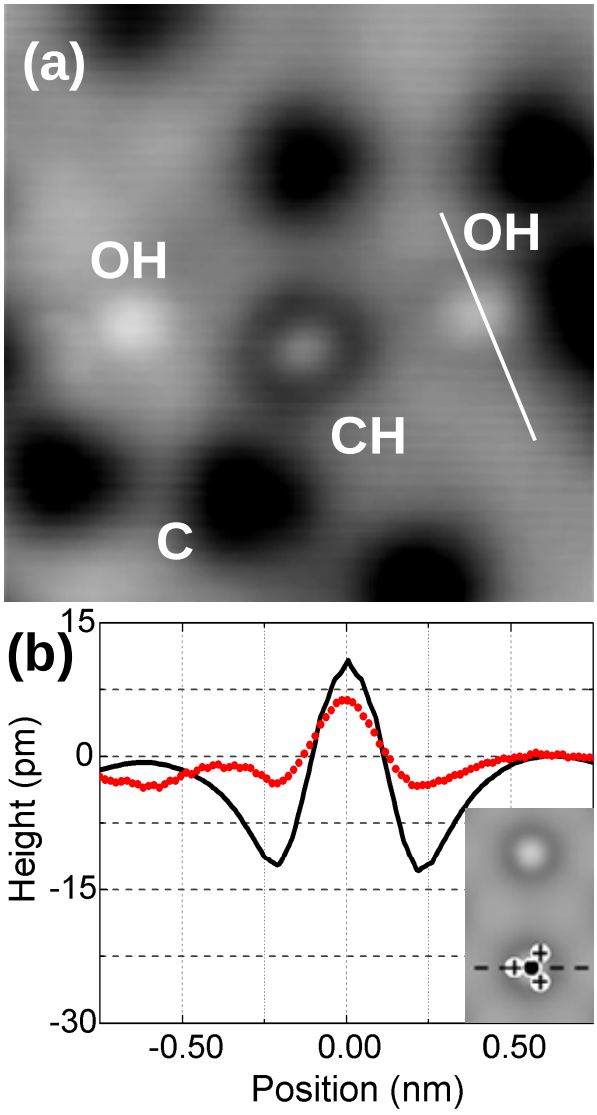

Figure 11.

5. Conclusions

Using a newly constructed low temperature STM we determined the species formed by the adsorption of H_2O, its dissociation, and reaction products on Ru(0001). Dissociation was produced by thermal annealing and also by tip-induced processes. The following surface species were identified by STM: O, C (present as an impurity atom), H_2O, H, CH, OH, H_2O-C complexes and H_2O-OH clusters. Identification could be accomplished by purely experimental methods, such as the direct adsorption of H_2 and O_2 molecules that are dissociated into H and O, or by tip-induced dissociation of species into its components as in the case of CH and OH.

We performed *ab initio* total energy calculations to identify adsorption sites and relative adsorption energies for each species. STM image simulations were then performed based on the DFT geometry. This provided an understanding of the origin of the STM contrast and greatly helped in the interpretation.

The library of fingerprint images of the various products thus established is a first and necessary step for any additional study based on STM of the mechanisms of water dissociation and other reactions on Ru. The results can be extended to other Pt group metals although differences in electronic states of different metals can probably change the absolute values of height or depth of each species. The trend in the apparent height of the various species, however, should remain the same; e.g., for metal terminated tips

water should always appear as a protrusion, while O, C and H as depressions of decreasing depth.

Acknowledgements. This work was supported by the Director, Office of Energy Research, Office of Basic Energy Sciences, Materials Sciences Division, of the U.S. Department of Energy under Contract No. DE-AC02-05CH11231. The theoretical work was supported by the Spanish Ministry of Science and Technology under Projects No. MAT2007-66719-C03-02 and NAN2004-09125-C07-06. The work of A.M. was financed by the Marie Curie Outgoing International Fellowship, Project No. 514412. Financial support from the Feodor Lynen Fellowship of the Alexander von Humboldt Foundation (M.H.) is gratefully acknowledged.

Figure Captions

Figure 1.

(a) Schematic diagram of the low temperature UHV STM system. (b) Cross-section and front view schematic of the microscope body. (c) A photograph of the microscope body inside the liquid He shield.

Figure 2.

Typical STM image (10 nm × 10 nm) of the as-prepared Ru(0001) surface. The surface contains approximately 0.03 ML of C atoms, imaged as 35-45 pm depressions visible as dark spots in a gray scale representation. The corrugation of the Ru atoms is too small to be visible. The C atoms are present as a result of segregation from the bulk during high temperature annealing. Tunneling conditions: 50 mV, 200 pA.

Figure 3.

(a) STM image (1.4 nm × 2 nm) of the Ru(0001) surface obtained with a sharp, single atom terminated tip. The Ru atoms, located at the weak maxima marked with red dots, have a corrugation of 2 pm in this image. The two large dark spots are due to C atoms. (b) STM image (3.5 nm × 5 nm) obtained after dosing a small amount of H_2 that modified the chemical nature of the tip apex. The corrugation of the Ru lattice is substantially enhanced with chemically modified tips. In this image the tip structure changed during the scan from an initial state (right side) to a more resolved one (center) and then back to its initial state. The corrugation of Ru lattice is 3 pm in the right and left area and 4-5 pm

in the middle. The same tip can produce 7-8 pm corrugation by using higher tunneling current. Tunneling conditions: (a) 21 mV, 100 pA; (b) 209 mV, 48 pA.

Figure 4.

Density of states (DOS) for the Ru(0001)-p(4 × 4)+H_2O system projected (PDOS) onto the H_2O molecule and the Ru atom below it. Dashed lines are the SIESTA PDOS and solid lines show the results of extended Hückel theory (EHT) fits. The molecular orbital (MO) decomposition of the H_2O PDOS is also shown. Top views of the gas phase MOs and their respective energies are sketched at the bottom of the figure. The percentages below the MO charge density plots give the relative contribution of each orbital to the tunneling current when the tip is on top of the molecule. The other 32% corresponds to the contribution from surrounding Ru atoms.

Figure 5.

(a)-(b) STM images (1.8 nm × 1.8 nm) of O and C atoms on Ru(0001) imaged with a blunt tip (a) and a sharp tip (b). With a blunt tip O and C are imaged as similar circular

depressions. With sharp tips O appears circular while the C shape is a rounded triangle. (c)-(d) Experimental height profiles (dotted red or blue curve) along the lines indicated in (b) together with simulated images (inset) and profiles (solid black curves) of C and O at the hcp hollow site. The + symbols in the simulated images mark the positions of the underlying Ru atoms. Note that the dip at around –0.6 nm in the experimental O profile is not related to atomic O, but is due to another species present nearby. Tunneling conditions: (a) 50 mV, 200 pA; (b)-(d) 45 mV, 260 pA.

Figure 6.

(a) STM image (8.5 nm × 10 nm) of Ru (0001) with ~0.03 ML of C atoms (dark spots) after adsorption of ~0.004 ML of H_2O at 25 K. The brighter protrusions are isolated H_2O monomers and the less bright features are water monomers bound to C atoms. (b) Cross section along the line in (a) through an isolated and a C-bound water molecule. Note that the C associated with the C-bound H_2O is not the one on the left, but on the upper side, which is almost invisible due to the overlap with H_2O and also due to the blunt tip. (c) STM image (2.3 nm × 3 nm) of an isolated H_2O molecule. (d) Simulated image of isolated top-site molecules. (e) Experimental (red dotted) and theoretical (black solid) height

profiles of the isolated H_2O monomer from (c) and (d). Tunneling conditions: (a) 50 mV, 200 pA; (c) 50 mV, 100 pA.

Figure 7.

STM images (3.7 nm × 3.7 nm) obtained (a) before and (b) after displacement of an H_2O molecule (bright) from one C atom (dark) to another. (c) Height profiles along the lines indicated in (a) and (b). In this way we can determine the actual distance between the center of C and H_2O features in the complex, to be 0.31 nm. (d) Proposed model of the H_2O-C complex. (e) Simulated images of a H_2O-C complex, and (f) of isolated H_2O and C (C on hcp hollow site, H_2O at the fourth nearest top site). (g) Theoretically calculated height profiles along the lines in (e) (black solid) and (f) (blue dotted). Tunneling conditions: (a) and (b): 23 mV, 990 pA.

Figure 8.

(a) STM image (2.25 nm × 2.25 nm) showing an isolated H atom, C atoms, and CH species on Ru(0001). (b) Observed (red dotted) and calculated (black solid) height

profiles through the H atom along the line indicated in (a) Inset: simulated image for H at fcc hollow site. Tunneling condition: 10 mV, 500 pA.

Figure 9.

STM images (1.75 nm × 1.75 nm) showing C (upper left) and CH species (other three) on Ru (0001) imaged with a blunt tip (a) and a sharp tip (b). The blunt tip images C as circular 45 pm depression and CH as a shallower 25 pm depression. With atomically sharp tips C appears as a triangular depression of similar depth, while CH appears as a triangular depression with a maximum at the center. (c) Experimental height profiles (red dotted) of the line indicated in (b) together with the theoretically derived profile (black solid). Inset: simulated CH at an hcp hollow site. The + symbols in the simulated images mark the positions of the underlying Ru atoms. Tunneling conditions: (a) 10 mV, 0.79 nA; (b) 9.5 mV, 0.79 nA.

Figure 10.

(a) STM image (9 nm × 9 nm) of a Ru(0001) surface after introducing water at 180 K. Clusters of mixed H_2O and OH (bright regions), coexist with CH species and C and H

atoms. The difference between C and CH is difficult to determine in this image because of the tip condition. (b) same region after repeatedly scanning over the cluster on the right at a sample bias of 0.5-0.7 V. This separated the components of the cluster in its lower half, revealing isolated O, H_2O, and OH. During this process, the tip apex changed and became atomically sharp. Tunneling conditions: 9 mV, 500 pA.

Figure 11.

(a) STM image (2.6 nm × 2.6 nm) showing two OH near CH and C. (b) Experimental height profiles (red dotted) of the line indicated in (a) together with the theoretically derived profile (black solid). The + symbols in the simulated images mark the positions of the underlying Ru atoms. Inset: simulated image of OH at an hcp hollow site. Tunneling condition: 24mV, 490 pA.

Table 1.

DFT derived adsorption energies [eV] for all the species considered in this work and for different high symmetry sites.

Footnote:

The calculations have been performed for a p(4 × 4) cell and the quoted values correspond to the total energy difference between the isolated gas-phase species plus the clean Ru(0001) p(4 × 4) slab and the adsorbed species including the Ru slab.

a) H_2O-C complex with the geometry depicted in Figure 7 (d): H_2O at top and C at hcp sites. The gas phase contribution to the adsorption energy is assumed to be the same as the sum of the isolated C and H_2O: 9.75 eV. Hence, the difference between the adsorption energies is an estimate of the strength of the H-C hydrogen bond, for which we obtain a value of 100 meV.

b) A metastable minimum in the total energy at this site was not found. Upon relaxing, the water molecule shifted to the top site.

Table 2.

Summary of adsorption sites, apparent height and shape in STM images obtained with blunt and sharp tips.

Footnote:

a) Theoretically derived appearances are shown only for the sharp tip.

REFERENCES

(1) Thiel, P. A.; Madey, T. E. *Surf. Sci. Rep.* **1987**, 7, 211-385 and references therein.

(2) Henderson, M. A. *Surf. Sci. Rep.* **2002**, 46, 5-308 and references therein.

(3) Ho, W. *J. Chem. Phys.* **2002**, 117, 11033-11061.

(4) Fomin, E.; Tatarkhanov, M.; Mitsui, T.; Rose, M. K.; Ogletree, D. F.; Salmeron, M. *Surf. Sci.* **2006**, 600, 542-546.

(5) Morgenstern, K.; Gawronski, H.; Mehlhorn, M.; Rieder, K.-H. *J. Mod. Opt.* **2004**, 10, 2813-2819.

(6) Hofer, W.A. *Prog. Surf. Sci.* **2003**, 71, 147-183.

(7) Tilinin, I. S.; Rose, M. K.; Dunphy, J. C.; Salmeron, M.; Van Hove, M. A. *Surf. Sci.* **1998**, 418, 511-520.

(8) CryoVac GmbH & Co KG, Heuserweg 14 D-53842 Troisdorf, Germany

(9) Pan, S. H.; Hudson, E. W.; Davis, J. C. *Rev. Sci. Instrum.* **1999**, 70, 1459-1463.

(10) Cerdá, J.; Soria, F. *Phys. Rev. B* **2000**, 61, 7965-7971.

(11) Cerdá, J.; Van Hove, M. A.; Sautet P.; Salmeron, M. *Phys. Rev. B* **1997**, 56, 15885-15899; www.icmm.csic.es/jcerda

(12) Soler, J.M.; Artacho, E.; Gale, J.; García, A.; Junquera, J.; Ordejón, P.; Sánchez-Portal, D. *J. Phys. Condens. Matter.* **2002**, 14, 2745-2779.

(13) Perdew, J. P.; Burke, K.; Ernzerhof, M. *Phys. Rev. Lett.* **1996**, 77, 3865-3868.

(14) Kostov, K. L.; Widdra, W.; Menzel, D. *Surf. Sci.* **2004**, 560, 130-144.

(15) Thiel, P. A.; Hoffmann, F. M.; Weinberg, W. H. *Phys. Rev. Lett.* **1982**, 49, 501-504.

(16) Wheeler, M. C.; Seets, D. C.; Mullins, C. B. *J. Chem. Phys.* **1996**, 105, 1572-1583.

(17) Bottcher, A.; Niehus, H. *J. Chem. Phys.* **1999**, 110, 3168-3175.

(18) Bocquet, M.-L.; Cerdá, J. ; Sautet, P. *Phys. Rev. B* **1999**, 59, 15437-15445.

(19) Blanco, J. M.; González, C.; Jelínek, P.; Ortega, J.; Flores, F.; Pérez, R.; Rose, M.; Salmeron, M.; Méndez, J.; Wintterlin, J.; Ertl, G. *Phys. Rev. B* **2005**, 71, 113402.

(20) Calleja, F.; Arnau, A.; Hinarejos, J. J.; de Parga, A. L. V.; Hofer, W. A.; Echenique, P. M.; Miranda, R.; *Phys. Rev. Lett.* **2004**, 92, 206101.

(21) Faradzhev, N. S.; Kostov, K. L.; Feulner, P.; Madey, T. E.; Menzel, D. *Chem. Phys. Lett.* **2005**, 415, 165-171.

(22) Clay, C.; Haq, S.; Hodgson, A. *Chem. Phys. Lett.* **2004**, 388, 89-93.

(23) Sautet P. ; Bocquet, M.-L. *Phys. Rev. B* **1996**, 53, 4910-4925.

(24) Mitsui, T.; Rose, M. K.; Fomin, E.; Ogletree, D. F.; Salmeron, M. *Science* **2002**, 297, 1850-1852.

(25) Komeda, T.; Fukidome, H.; Kim, Y.; Kawai, M.; Sainoo, Y;. Shigekawa, H. *Jpn. J. Appl. Phys.* **2002** 41, 4932-4935.

(26) Morgenstern, K.; Rieder, K.-H. *J. Chem. Phys.* **2002**, 116, 5746-5752.

(27) Michaelides, A.; Alavi, A.; King, D. A. *J. Am. Chem. Soc.* **2003**, 125, 2746-2755.

(28) Isaacs, E. D.; Shukla, A.; Platzman, P. M.; Hamann, D.R.; Barbiellini, B.; Tulk, C.A. *Phys. Rev. Lett.* **1999**, 82, 600-603.

(29) Feibelman, P. J. *Surf. Sci.* **1987**, 179, 153-162.

(30) Lindroos, M.; Pfnur, H.; Feulner, P.; Menzel, D. *Surf. Sci.* **1987**, 180, 237-251.

(31) Sokolowski, M.; Koch, T.; Pfnur, H. *Surf. Sci*. **1991**, 243, 261-272.

(32) Tatarkhanov, M.; Rose, F.; Fomin, E.; Ogletree, D. F.; Salmeron, M. *Surf. Sci.* **2007**, in press; doi:10.1016/j.susc.2007.10.042